Physiological stress response associated with elevated CO_2 and dissolved iron in a phytoplankton community dominated by the coccolithophore *Emiliania huxleyi*

María Segovia[1,*], M. Rosario Lorenzo[1], Concepción Iñiguez[1], Candela García-Gómez[1,2]

[1]Department of Ecology, Faculty of Sciences, University of Málaga, Bulevar Louis Pasteur s/n, 29071 Málaga, Spain

[2]Present address: Spanish Oceanographic Institute (IEO), Puerto Pesquero, 29640 Fuengirola, Málaga, Spain

ABSTRACT: We exposed a natural phytoplankton community to combined present (390 µatm, low carbon [LC]) and future CO_2 levels predicted for the year 2100 (900 µatm, high carbon [HC]), and ambient (4.5 nM, −DFB [desferoxamine B]) and high (12 nM, +DFB) dissolved iron (dFe) levels, for 25 d in mesocosms. We report on the physiological response of the community dominated by the coccolithophore *Emiliania huxleyi*. The community structure shifted on Day 10, leading to 2 different phases (1 and 2), i.e. before and after Day 10, respectively. We focussed on the massive bloom of *E. huxleyi* that developed in Phase 2, in the LC+DFB treatment. In high dFe conditions, pigments and photosynthetic parameters increased compared to the control (LC−DFB). Cell death was only detected during the community shift (Days 10−12) and mostly increased in the presence of high CO_2. The accumulation of reactive oxygen species (ROS) decreased under high dFe, pointing to an efficient, rather than a stressed, metabolism. DNA lesions, caused by excess irradiance, were minimised under high Fe. *E. huxleyi* is known for its low Fe requirements for growth. However, we demonstrate that Fe is essential to *E. huxleyi* for DNA repair and ROS management, and to maintain optimal functioning of the photosynthetic machinery, with implications for carbon cycling and future ecosystem functioning.

INTRODUCTION

Anthropogenic activities are resulting in a progressive enhancement of atmospheric CO_2 towards levels predicted to reach up to 900 µatm by the year 2100 (Stocker et al. 2013). The increase in atmospheric CO2 levels are already affecting the oceans at an unprecedented rate, by decreasing seawater pH (ocean acidification) and also the calcium carbonate saturation state (Beardall et al. 2009, Doney et al. 2009). Earth system models project a global additional decrease in pH by the year 2100 ranging from 0.06 to 0.32 units, depending on our future emissions (Ciais et al. 2013), on top of the current decrease of 0.1 units since the beginning of the industrial era. In addition, concomitant global warming may enhance stratification, reducing nutrient availability and increasing irradiance due to a shallower thermocline (Boyd & Doney 2002). A quarter of the CO_2 emitted to the atmosphere has been absorbed by the oceans since the beginning of the Anthropocene (Sabine et al. 2004). However, most of the dissolved CO_2 remains above the permanent

thermocline, and up to 30% remains in the upper 200 m of the water column, unequivocally affecting physiological processes (Sabine et al. 2004).

Ocean acidification thus directly impacts biogeochemistry, subsequently affecting bioactive trace metal solubility and speciation (Millero et al. 2009). Trace metals are required for a broad range of physiological processes in phytoplankton. Iron (Fe) in particular is the most quantitatively important transition metal in marine phytoplankton (Twining & Baines 2013). It is involved in numerous cellular functions and in fundamental metabolic pathways, controlling growth. Above all, it is crucial because of the many Fe-dependent electron transport components in photosynthetic membranes (Behrenfeld & Milligan 2013). Therefore, changes in Fe bioavailability have profound effects on phytoplankton growth and biomass, ultimately affecting carbon fluxes in marine systems (for a review, see Marchetti & Maldonado 2016). In oxygenated seawater, without organic complexation, Fe is usually complexed to hydroxides. Hence, a decrease in pH will increase Fe(III) solubility and prevent Fe(II) from binding to carbonate (Millero et al. 2009), as the carbonate ion would be reduced by 54% at low pH (Beardall et al. 2009). However, in the presence of strong organic ligands, increased CO_2 in seawater decreases Fe bioavailability to phytoplankton (Shi et al. 2010). Elevated CO_2 also affects phytoplankton physiology and growth (Mackey et al. 2015). Field experiments have shown mixed responses to alteration in CO_2 and Fe concentrations within natural phytoplankton assemblages from high nutrient–low chlorophyll regions (Marchetti & Maldonado 2016). Fe availability increased as a result of CO_2 enrichment in a mesocosm experiment in the same fjord where our experiment was carried out (Breitbarth et al. 2010). In contrast, decreases in Fe uptake rates, Fe availability and growth of phytoplankton with increasing CO_2 levels were observed in the North Atlantic and the Bering Sea (Marchetti & Maldonado 2016).

Coccolithophores are among organisms heavily affected by CO_2 (Riebesell & Tortell 2011 and references therein). The majority of coccolithophores reduce their level of calcification when growing at increased CO_2. Furthermore, the fossil record suggests that eras with reduced CO_2 levels (e.g. glacial maxima) have favoured more heavily calcified cells (Beaufort et al. 2011). Elevated CO_2 may act as a stressor to coccolithophores due to problems related to calcification leading to thinner coccospheres (Mackey et al. 2015). When combined with other stressors, such as an excess of photosynthetically active radiation (PAR) and ultraviolet radiation (UVR) irradiances, high CO_2 may exert enhanced harming effects in cells with insufficient calcium carbonate (Gao et al. 2009, Xu et al. 2011). Excess irradiance injures phytoplankton by inducing photobleaching of photosynthetic pigments and by altering complexes and molecules present in the photosynthetic apparatus such as the Photosystem II (PSII) complex and/or the rubisco enzyme (Häder et al. 1998). However, the cells react to high light conditions by triggering photoprotection mechanisms (Segovia et al. 2015 and references therein). The most important ones are related to the xanthophyll cycle (oxygenated carotenoids), and other carotenoids regarding non-photochemical quenching (NPQ). The violaxanthin–anteraxanthin–zeaxanthin (VAZ) cycle has been described in chlorophytes, and the

diadinoxanthin–diatoxanthin (DD–DT) cycle is present in Bacillariophyceae, Haptophyta, and most of the chl *c* containing algae (Takaichi 2001).

Apart from photodamage and photoinhibition of photosynthesis, exposure of cells to high light causes DNA damage by means of cyclobutane pyrimidine dimer (CPD) formation, which constitutes the major class of these lesions found in phytoplankton (Buma et al. 2000). High irradiance also leads to the generation of reactive oxygen species (ROS) that can affect several molecular targets in the cells and are responsible for the inhibition of repair in the damaged DNA and photosynthetic machinery (Lesser 2006). Hence, any process involved in minimising photodamage and DNA damage and helping to overcome the oxidative burst is crucial for stress management and survival (García-Gómez et al. 2014, 2016, Segovia et al. 2015).

In a previous companion publication from this mesocosm experiment studying the whole plankton food web (Segovia et al. 2017), we showed that the biomass of the coccolithophore *Emiliania huxleyi* was negatively affected by increased CO_2, and positively affected by an increase in dissolved Fe (dFe), suggesting *in situ* Fe limitation. However, increased dFe partially mitigated the negative effect of elevated CO_2, indicating that *E. huxleyi* was able to acclimate better to ocean acidification when Fe availability was high. The underlying physiological acclimation response in the studied *E. huxleyi* strain to stress caused by ocean acidification is actually unknown, but it may be tightly regulated by Fe. Fe is required for many metabolic processes, including carbon and nitrogen fixation, nitrate and nitrite reduction, chlorophyll synthesis and the electron transport chains of respiration and photosynthesis. Fe is also incorporated into several enzymes that deal with ROS (Twining & Baines 2013), and in some of the enzymes that participate in DNA repair (Lukianova & David 2005, Morita et al. 2010).

Despite the considerable contribution of marine phytoplankton to global climate and biogeochemical cycles, many aspects of their physiology in future global change–ocean biology relationships are poorly understood. Direct field studies on natural phytoplankton communities using mesocosm experiments aiming to unravel the relevance of future environmental conditions are required to assess the impacts of global change on phytoplankton. This will allow us to better predict the functioning and composition of the future ocean under a multiple-stressor scenario (Riebesell & Gattuso 2015).

The work we present here builds on our previous companion study (Segovia et al. 2017). The novelty of this study consists in unravelling the physiological response of only phytoplankton, and specifically *E. huxleyi*, regarding stress management. Thus, the aim of this work was to investigate the effect of increased CO_2 and Fe availability on the physiological response of the different phytoplankton groups during a natural phytoplankton bloom of the coccolithophore *E. huxleyi*, using mesocosms. Specifically, we analysed the impact of the stressors on: (1) performance of the thylakoidal transport chain, (2) content and function of pigments, (3) cell viability/cell death, (4) oxidative stress and (5) accumulation of DNA damage. *E.*

huxleyi is the keystone of the coccolithophores (Paasche 2001, Hutchings 2011). It is a globally relevant species, playing a major role in the global carbon cycle by regulating the exchange of CO_2 across the ocean–atmosphere interface through photosynthesis and calcium carbonate precipitation (Rost & Riebesell 2004). *E. huxleyi* is sensitive to elevated CO_2 (Riebesell & Tortell 2011) and apparently has low Fe requirements (Muggli et al. 1996).

This study is the first to analyse the physiological stress responses of *E. huxleyi* and other phytoplankton species in a mesocosm experiment where CO_2 and dFe concentrations were simultaneously manipulated.

MATERIALS AND METHODS

Experimental design

A mesocosm experiment was carried out in the Raunefjord (60.39° N, 5.32°E) off Bergen, Norway, from 5–27 June 2012, as described by Segovia et al. (2017). Twelve mesocosms (11 m^3 each) were set up in a full factorial design with all combinations of ambient and high partial pressure of CO_2 (pCO_2) and 2 treatments of dFe in 3 independent replicate mesocosms per treatment. High-density polyethylene mesocosms were filled with fjord water pumped from 8 m depth.

They were covered with low-density polyethylene lids in order to avoid pCO_2 losses and contamination. Mesocosms and their lids were transparent to PAR and UVR (UVA + UVB). After the first sampling day (Day 0), the seawater of half of the mesocosms was enriched with CO_2 (Schulz et al. 2009) to achieve high pCO_2 concentrations corresponding to levels predicted for the year 2100 (900 µatm, high carbon [HC]; Stocker et al. 2013) and the other half were not manipulated (ca. 390 µatm, low carbon [LC]; see Fig. S1A in the Supplement at www.int-res.com/articles/suppl/m586p073_supp.pdf). All mesocosms were continuously and gently mixed by using an airlift system (Egge & Heimdal 1994). For the CO_2 enrichment, 150 l of fjord water were aerated with pure CO_2 at a flow rate of 1.5 l min^{-1} overnight and added to each of the mesocosms belonging to the HC treatments. To maintain the pCO_2 in the HC treatments, ambient air was mixed with pure CO_2 at a flow rate of 200 ml min^{-1}, and the enriched mixture (900 µatm CO_2) was pumped directly to the airlift system. The LC treatment consisted of only ambient air similarly connected. High efficiency particulate air (HEPA) filters were placed between the air pumps and the airlift system to avoid particulate contamination. Mesocosms were fertilised after the initial sampling (Day 0) by addition of 10 µM nitrate and 0.3 µM phosphate to induce a bloom of the coccolithophore *Emiliania huxleyi* (Egge & Heim dal 1994). To promote changes in Fe availability, and analyse its effects on the phytoplankton community, 70 nM (final concentration) of the siderophore desferoxamine B (DFB) (+DFB and −DFB treatments) was added to half of the mesocosms on Day 7, when the community was already acclimated to high CO_2. Even though DFB is a strong Fe-binding organic ligand often used to induce Fe limitation in phytoplankton (Wells 1999), DFB

additions may also increase the dFe pool in environments with high concentrations of colloidal and/or particulate Fe, such as fjords (Kuma et al. 1996, Öztürk et al. 2002). Thus, the DFB addition promoted high (12 nM, +DFB) dFe levels vs. ambient (4.5 nM, −DFB) dFe concentrations (Segovia et al. 2017) (Fig. S1B). The multifactorial treatments were thus LC−DFB (control), LC+DFB, HC+DFB and HC−DFB. Water samples from each mesocosm were taken from 2 m depth by gentle vacuum pumping of 25 l into acid-washed carboys that were quickly transported to the onshore laboratory. All variables were analysed on a daily basis and/or every other day, unless otherwise indicated.

Irradiance and temperature

Solar spectral irradiance comprising PAR wavelengths (400−700 nm), UVA (320−400 nm) and UVB (280−320 nm) was recorded at 2 m depth (sampling depth) in mesocosm 3 (belonging to the LC−DFB treatment) at 5 min intervals during the experiment, by using a Trios Ramses spectroradiometer. HOBO Pendant Temperature/Light loggers (Onset Computer) were attached to the airlift system in 1 mesocosm of each treatment group at depths of 0, 1, 2 and 3 m and at the surface in air, to ensure that mesocosms received the same irradiance as well as to monitor irradiance profiles and water temperature. The equivalent biologically effective irradiances were calculated using the biological weighting functions for chloroplast inhibition (Jones & Kok 1966), general plant damage (Caldwell 1971), DNA damage (Setlow 1974), inhibition of phytoplankton photosynthesis (Cullen et al. 1992), and inhibition of photosynthesis in Antarctic phytoplankton (Cullen & Neale 1997). These data are summarized in Table 1.

Phytoplankton abundance and biomass

Phytoplankton <20 µm was analysed using a FACSCalibur flow cytometer (Becton Dickinson) according to Marie et al. (1999) and Larsen et al. (2001). Phytoplankton >20 µm and microzooplankton were analysed with a FlowCAM following Jakobsen & Carstensen (2011). Abundances of all groups were converted into carbon biomass following Menden-Deuer & Lessard (2000) and Olenina et al. (2006). For detailed information, see Segovia et al. (2017).

Pigments

Samples (1 to 2 l) were collected from each mesocosm and gently filtered through GF/F filters, snap frozen in liquid nitrogen and kept at −80°C until analysis. Pigments were extracted using N, N-dimethylformamide overnight at 4°C. Chlorophyll a (chl *a*) concentration was determined spectrophotometrically and was calculated according to Wellburn (1994). The carotenoids Lutein (LUT), neoxanthin (NEO), violaxanthin (V), anteraxanthin (A), zeaxanthin (Z), peridinin (PERI), fucoxanthin (FUCO), 19'-butanoyloxyfucoxanthin (BUTA), 19'-hexanoyloxyfucoxanthin (HEXA), diadinoxanthin (DD), diatoxanthin (DT), prasinoxanthin (PRAS), pheophorbide (PHEO) chlorophyllide a (Chlide), chl c_3 and chl c_2 were determined by HPLC as described by Lubian & Montero (1998). The pigmentary ratios DT+DD:TFUCO (total

FUCO) and HEXA:TFUCO were used as proxies for the cellular physiological status and nutrient limitation, respectively, of *E. huxleyi* cells in multispecific bloom situations (Stolte et al. 2000).

In vivo chl *a* fluorescence

Optimal quantum yield (F_v/F_m) of PSII was measured in 10 min dark-adapted samples by pulse amplitude modulated fluorometry (Water-PAM, Walz). Rapid light curves were constructed according to Figueroa et al. (2009) and fitted to the model of Eilers & Peeters (1988) to obtain the initial slope (α) and the relative maximal electron transport rate($rETR_{max}$). The light saturation parameter (E_k) was derived from $rETR_{max}$ and α.

Cell viability

Cell viability was assessed using the nucleic acid stain SYTOX green (Invitrogen) according to Segovia & Berges (2009). SYTOX green only stains the nucleic acid of cells that have compromised plasma membranes. Green staining of the cell nucleus indicates a dead cell before the cell loses its integrity and lyses (Veldhuis et al. 2001), while viable cells are not stained and fluoresce in red. Samples from each mesocosm (1–2 l) were concentrated by gentle filtration under low pressure onto 0.8 µm, 47 mm polycarbonate membranes to a final volume of 15 ml at 10°C. Chl *a* content in the concentrates was measured by extraction in 90% acetone overnight and determined fluorometrically using a Turner fluorometer 10-AU (Turner BioSystems). Final chl *a* concentration in cell concentrates ranged from 0.2 to 400 µg l^{-1}. SYTOX green (5 µM final concentration) was added to 1 ml of the concentrated cell suspensions from the natural phytoplankton community. Samples were incubated at 10°C (natural temperature condition in the fjord) in darkness for 60 min. Fluorescence was quantified in a Nikon epifluorescence microscope at an excitation of 490 nm and an emission of 525 nm. Between 30 and 50 fields of view were analysed per sample (N ≥ 600). Positive controls consisted of 100% killed cells, which were run in parallel and obtained by pretreating the samples with 1% glutaraldehyde (final concentration) for 2 h at 4°C.

General oxidative stress

The intracellular accumulation of ROS was assayed in concentrated cell suspensions from the natural phytoplankton community (as above) according to Segovia & Berges (2009) and Bouchard et al. (2013). In brief, cells were incubated with 10 µM carboxy-H2DFFDA (final concentration; Invitrogen) at 10°C for 90 min in darkness. Fluorescence was quantified in a Nikon epifluorescence microscope at an excitation of 490 nm and an emission of 525 nm. Between 30 and 50 fields of view were analysed per sample (N ≥ 600). DNA damage DNA damage was assessed according to García-Gómez et al. (2012). Samples (1 to 2 l) were collected from each mesocosm and gently filtered through 0.8 µm polycarbonate filters. Samples were snap frozen in liquid nitrogen and kept at −80°C until analysis. For analysis, DNA was extracted and quantified from the filters; 15 ng of DNA were used from each sample

for immunodetection of CPDs with a monoclonal anti-CPD antibody (H3, Affitech). Positive controls consisted of UVR-radiated DNA from *Dunaliella tertiolecta* and lambda phage (García-Gómez et al. 2014). Negative controls consisted of the same DNA sample species without radiation. Unspecific cross-reactivity controls were carried out by incubating the membranes with only the secondary antibody in the absence of the primary antibody. The signal was detected by chemiluminescence (ECL, GE Healthcare), and the intensity of cross-reactions was quantified in a Gel Logic Image Analyser (Eastman-Kodak).

Statistical analyses

Data were checked for normality (by Shapiro-Wilks' test), homoscedasticity (by Cochran's and Levene's tests) and sphericity (by Mauchly's and/or Bartlett's tests). Variables met all criteria to perform parametric tests. Statistical significance of treatment effects on variables was performed using split-plot ANOVA (SPANOVA or mixed-model ANOVA) followed by post hoc Sidak or Tukey and Bonferroni tests, respectively (considering $p < 0.05$ and/or $p < 0.01$ as significant). When appropriate, data were specifically tested for significant differences ($p < 0.05$) induced by the treatments by using 1- or 2-way ANOVAs and/or Student's t-tests, as well as Pearson's product-moment correlations. All analyses were performed using the general linear model procedure with main effects (CO_2, dFe), time (repeated measure) and all interactions. The weighted importance of the environmental factors (pCO_2 and dFe) on the measured biological responses was also assessed by means of principal component analysis. Statistical analyses were performed using the software Statistica v12 (Statsoft), SPSS v22 (IBM statistics) and PAST v3.14 (Hammer et al. 2001).

RESULTS

Irradiance and temperature

Meteorological conditions during the experiment were stable with 75% clear sky days and 25% partly cloud covered days. Average (± range) midday (solar noon ± 2 h) irradiance in the mesocosms at 2 m depth was 276.17 (±44.8) µmol photons m^{-2} s^{-1} PAR; 1.61 (±0.98) W m^{-2} UVA; and 0.01 (±0.011) W m^{-2} UVB. The midday average irradiance varied around this mean on days with cloud cover. Experimental irradiances and corresponding weighted irradiances (i.e. biological effective irradiance), as well as the biological effective dose calculated for the control mesocosms are shown in Fig. 1 and Table 1. Irradiance and transmittance through polyethylene mesocosms and lids are shown in Table S1 in the Supplement. The water temperature in the mesocosms varied between 10 and 11°C, corresponding to the surrounding fjord temperature.

Increased CO_2 and Fe availability promote a shift in the phytoplankton community structure

Pigment composition was dependent on the shifts in the phytoplankton community during the experiment, as already reported by Segovia et al. (2017, see Fig. S1). Two phases were observed during the experiment: Phase 1 comprised Days 0–10, and Phase 2 spanned Days 11–22.

Briefly, in Phase 1, the mesocosms were filled with water from the fjord where an intense diatom bloom was occurring, mainly comprised of long chain forming diatoms (*Skeletonema* sp., *Thalassiosira* spp., *Chaetoceros* spp. and other diatoms; Fig. S2F). This diatom bloom declined in the mesocosms by Day 7 of the experiment. Other phytoplankton groups peaked between Days 3 and 5 and declined sharply after Day 5, namely picoeukaryotes (Fig. S2C), small nano eukaryotes likely composed small prasinophytes and small haptophytes (Fig. S2D), and large nanoeukaryotes like single-celled diatoms and flagellated forms (Fig. S2E). Microplankton, such as dinoflagellates (dominated by *Gyrodinium* spp. and *Ceratium* sp. and less abundant species such as *Protoperidinium* spp., *Dinophysis* spp. and *Prorocentrum* spp.; Fig. S2G), were also present, contributing significant biomass. *Synechococcus* sp. and *Emiliania huxleyi* were also present but did not grow significantly in this phase (Fig. S2A,B). Thus, the increase in chl *a* (Fig. S3) experienced due to these organisms' growth was masked by the declining microplanktonic diatoms, and, during Phase 1, there were no significant differences between treatments in species composition/proportions, nor in any of the pigment concentrations (Segovia et al. 2017).

In Phase 2, a bloom of the coccolithophore *E. huxleyi* was observed under LC+DFB conditions outcompeting all other phytoplankton groups. This bloom was not observed in the control treatment (LC−DFB) or in the HC treatments (Fig. S2A). *Synechococcus* abundance showed a similar response pattern to that of *E. huxleyi* but contributed to the total chl *a* with very low biomass (Figs. S2B & S3). Picoeukaryotes, small and large nanoeukaryotes and microphytoplankton were not affected by changes in CO_2, dFe levels or their interaction. Hereafter, we focus on Phase 2, which is the time frame corresponding to the coccolithophore's main contribution to all physiological variables measured. However, data corresponding to Phase 1 and the shift-point are also presented in order to understand the phytoplankton succession occurring in the mesocosms.

Increased dFe modulates the accumulation of pigments at different pCO_2 levels

In Phase 2, high pCO_2 negatively affected the concentrations of all pigments (Table 2), while increased dFe (+DFB) had a general positive effect. However, this positive Fe effect was stronger in LC when compared to the HC treatments (Fig. 2A–D, Table 2). Chl c_2 and chl c_3, DD and HEXA exhibited similar patterns, reaching their highest concentrations in LC+DFB, followed by LC−DFB and HC treatments. DT showed differences only on Day 19 due to both factors (Fig. 2E, Table 2), when the control was significantly higher than the rest of the treatments (post hoc Sidak, $p = 0.011$). FUCO and PERI concentrations increased from Day 14 onwards in the control (LC−DFB) and were significantly different from the rest of the treatments (Fig. 2F,G,

Table 2). PRAS and BUTA constantly increased in the LC treatments. Z was significantly higher in LC vs. HC from Day 14 onwards, regardless of Fe levels (Fig. 2J, Table 2); thus, its concentration was affected by pCO_2 but not by DFB or their interaction. Lut, Ne, V, A, Pheo and Chlide were not detected. The results obtained indicate that Fe was modulating the effect of pCO_2 on the pigment concentrations. The pigmentary ratios DT+DD:TFUCO and HEXA: TFUCO drastically changed during Phase 2. They were strongly affected by dFe and modulated by CO_2, since the interaction between both factors was significant (Fig. 3, Table 2).

Photosynthetic parameters are dependent on pCO_2 and dFe levels

During Phase 1 (Days 1–10), there were no significant differences between treatments in any of the photosynthetic parameters (Fig. 4). On Day 10, a transitory decrease in the photosynthetic efficiency (α, Fig. 4A) was observed. It followed the same trend as the optimum quantum yield (F_v/F_m, Fig. S4; Segovia et al. 2017). This transitory change was paralleled by an increase in the $rETR_{max}$ (Fig. 4B) and in the saturation irradiance (E_k, Fig. 4C) in all treatments. Between Days 11 and 22 (Phase 2), α matched the F_v/F_m trend, with the LC treatments showing higher values than the HC treatments after Day 12. High dFe (+DFB) had a significant positive effect on LC treatments, promoting a higher efficiency, while it did not exert any potential benefit in the HC treatments (Table 2). F_v/F_m was indeed significantly higher in the LC than in the HC treatments. High dFe (+DFB) promoted a significant increase in F_v/F_m in LC (LC+DFB) with respect to the control (LC−DFB; Table 2). In contrast, in the HC−DFB treatments, F_v/F_m increased due to the dominance of phytoplankton groups that were not affected by increased CO_2 such as small and large nanoeukaryotes and dinoflagellates (Fig. S1). Both pCO_2 and dFe, as well as their interaction, had significant effects on F_v/F_m in *E. huxleyi* and *Synechococcus* sp. during Phase 2 (Segovia et al. 2017; Fig. S4). $rETR_{max}$ and E_k were not significantly different between treatments in Phase 2.

Cell death is affected by high CO_2, and general oxidative stress decreases under high dFe

Cell death was not detected during the experiment except on Days 11 and 14 (Fig. 5A). On Day 11 under increased CO_2, 20% of the cells presented SYTOX-positive green fluorescence, indicating a complete loss of viability, i.e. cell death. In the LC treatments, there were 4-fold fewer green fluorescent labelled cells, indicating that HC had a significant negative effect on part of the phytoplankton population when compared to LC (Table 2). By Day 14, the percentage of SYTOX-positive cells decreased 10-fold to threshold levels. C-H_2DFFDA green fluorescence emitted by the cells due to general oxidative stress was significantly higher in HC than in LC at the beginning of the experiment, declining by 60% between Days 3 and 7. As was observed for cell death, ca. 20% of the cells showed symptoms of oxidative stress on Day 11 (Fig. 5B). However, in this case, the percentage of H_2DFFDA-green fluorescent labelled cells was significantly higher in ambient dFe (−DFB) than in high dFe grown cells (+DFB), regardless the CO_2 levels (Table 2).

DNA damage is minimised by increased dFe in *E. huxleyi*

In Phase 1, CPD formation significantly increased 4-fold between Days 1 and 3 (Fig. 6), and remained steady and with no differences between treatments up to Day 9 (Table 2). CPDs increased in cells exposed to high dFe (+DFB) on Day 9, whilst the treatment showing less DNA damage was HC−DFB. CPD content was drastically reduced between Days 9 and 11. As Phase 2 progressed, the treatments that exhibited significantly increased levels of accumulated DNA damage were those at ambient dFe (−DFB, Table 2). In contrast, after Day 11, the treatments with high Fe (+DFB) presented significantly lower CPD concentrations than the control, regardless of the CO_2. HC+DFB showed similar levels to the control, indicating a positive Fe effect counteracting CPD accumulation under increased CO_2.

DISCUSSION

In the present work we studied physiological processes related to photosynthesis, pigment production, oxidative stress, DNA damage and cell death, in order to understand the final response of the phytoplankton community and in particular, of the coccolithophore *Emiliania huxleyi*, to the interactive manipulation of CO_2 levels and Fe availability. Segovia et al. (2017) reported fluctuations in pCO_2 levels in the HC treatments. However, the targeted high CO_2 concentrations were achieved in the mesocosms although the steady state values were slightly lower (900 µatm) than target values (1000 µatm). Variations in pCO_2 between Fe treatments were due to a higher dFe solubilisation and thus increased productivity (see Segovia et al. 2017 for extensive details). The observed fluctuations are the result of the natural variability in seawater carbonate chemistry speciation, caused by changes in temperature and biological activities such as photosynthesis, respiration, nutrient utilisation, remineralisation and calcium carbonate precipitation and dissolution (Riebesell et al. 2008, Schulz & Riebesell 2013). Despite that, the reproducibility between the triplicates of each treatment was high, allowing us to isolate and identify single and interactive effects on the variables we measured.

The changes in these variables were assessed in relationship to the different functional phytoplankton groups that developed during the 3 distinct phases of the experiment (Segovia et al. 2017, Fig. S2 in the Supplement): (1) Phase 1 (Days 0−10), characterized by the absence of effects on the phytoplankton community and its response, (2) the shift-point (Day 10−11), when the phytoplankton community shifted due to mid-term effects of increased CO_2 and dFe levels, and (3) Phase 2 (Days 11−22), distinguished by an evident response of the community to treatment effects in the long term. A bloom of the coccolithophore *E. huxleyi* developed in Phase 2 under ambient CO_2 and increased dFe (LC+DFB), outcompeting the rest of the phytoplankton groups. This bloom was not observed in the control at ambient CO_2 and dFe (LC−DFB) nor in the high CO_2 conditions, although *E. huxleyi* was the most abundant species in all treatments except in HC−DFB (Fig. S2). Segovia et al. (2017) demonstrated that Fe concentrations may control phytoplankton community structure in coastal ecosystems, that ocean acidification can enhance dFe, and that in areas with high total Fe concentrations (particulate and dissolved), the

detrimental effects of increased pCO_2 on *E. huxleyi* can be partially mitigated by enhanced dFe. However, the physiological response behind this is unknown and the consequences of the interactive effects of pCO_2 and Fe availability on *E. huxleyi* can be critical to carbon cycling and marine ecosystems.

From a physiological point of view, Fe plays a major role in plankton ecology since several aspects of thylakoid electron transport and accessory pigments are Fe dependent. A decline in the cellular pigment content seems to be a general behaviour under Fe stress (Behrenfeld & Milligan 2013). The response shown by the community when dFe concentration increased (Segovia et al. 2017) demonstrated that *E. huxleyi* was experiencing Fe limitation in the control (LC− DFB), as reflected in decreased cell numbers and biomass relative to the other treatments (Fig. S2), as well as a lower chl *a* content (Fig. S3). The Fe demand calculated in Segovia et al. (2017) during the coccolithophore bloom confirmed the Fe limitation scenario for *E. huxleyi* and that the highest growth rates were obtained in the LC+DFB treatment, whilst slower growth took place in the treatments with ambient Fe and/or high HC. Cellular accumulation of pigments occurred during the phytoplankton community succession (Fig. 2) as reported in other experiments (Suffrian et al. 2008, Polimene et al. 2012). Pigment signatures are used to determine the contribution of the distinct taxonomic groups in natural assemblages. Accordingly, the distribution of pigments in our experiment is in agreement with the flow cytometry data (Segovia et al. 2017). Pigments changed specifically on Days 10−11, in parallel with a community shift observed in Phase 2 (Fig. S1). Chlorophylls, xanthophylls and fucoxanthins that were detected (Fig. 2) corresponded to Cyanophyta, Heterokontophyta, Haptophyta, Dinophyta and Chlorophyta (Takaichi 2001) present in the mesocosms.

However, what determines phytoplankton species fitness, succession and distribution are the physiological trade-offs between light harvesting, photoacclimation or photoprotection and dissipation of excess energy, in which all pigments participate. This is also reflected by changes in the pigment ratios of DT+DD:TFUCO and HEXA:TFUCO indicating physiological stress (Stolte et al. 2000). In Phase 2, chl c_2 and chl c_3 showed the highest concentrations and closely followed the same trend as *E. huxleyi* biomass (Fig. S1). They are considered secondary chlorophylls especially found in light-harvesting complexes. Due to their distribution in these complexes, the function of chl *c* in *E. huxleyi* photosynthesis has been described as an enhancement of light absorption, particularly in the blue wavelength (Mizoguchi et al. 2011). The xanthophyll DD−DT cycle was probably active, playing a key role in NPQ (the nonradiative dissipation of excess of energy reaching the photosynthetic apparatus; Demmig-Adams & Adams 1996). However, the VAZ cycle was most likely not active, because only Z accumulated in Phase 2 (Fig. 2). HEXA, FUCO and PRAS peaked in Phase 2 in the treatments with the highest biomass accumulation (LC+DFB). These pigments possess light-harvesting functions and are highly efficient at transferring energy to chlorophylls (Stolte et al. 2000), which is essential for efficient utilisation of available light at wavelengths not 'harvested' by chlorophyll. All pigments were significantly negatively affected by CO_2 levels, and some were positively affected by dFe (Table 2).

In multi-species bloom situations, the ratio of DT+DD:TFUCO can be used as an indicator of the cellular physiological status of *E. huxleyi* (Stolte et al. 2000), instead of using the ratio DT+DD:chl *a*, which also accounts for other taxonomic groups present. Increased HEXA:TFUCO ratios have been observed in nutrient-limited *E. huxleyi* due to reduced growth (a similar nutrient scenario as in this experiment, Segovia et al. 2017). We observed the highest HEXA:TFUCO ratios (mol:mol) under LC+DFB, followed by HC+DFB treatments (Fig. 3A), always well above the control (LC−DFB) and HC−DFB treatments. HEXA also has light-harvesting functions in *E. huxleyi* (Stolte et al. 2000); hence, HEXA is most likely increasing the antenna size, and possibly the number of reaction centres. This points to a constrained physiological status of the cells at ambient dFe concentration (LC−DFB), and to a benefit of high dFe effects for the cells under HC. In agreement, the other functional ratio (DT+DD):TFUCO was higher at high dFe concentrations relative to the control (Fig. 3B) and regardless of CO_2 levels. Thus, in the control, a lower (DT+DD):TFUCO (mol: mol) ratio implies a dilution of the DD−DT cycle, meaning that the cells' capacity for NPQ is decreased, being prone to photodamage. Indeed, Fe-limited cells show a high susceptibility to photooxidation (Behrenfeld & Milligan 2013).

The functional ratios showed that the performance of the above-mentioned pigments was higher under increased Fe levels. This leads to a better functioning of the photosynthetic electron transport chain, although CO_2 could modulate this effect (Table 2). Although some field studies have shown that F_v/F_m is unaffected by increased CO_2 levels (Endo et al. 2013, 2017, Sugie et al. 2013), in our experiment, photosynthetic parameters were significantly affected by both CO_2 and Fe levels in Phase 2. On Day 10, a transitory decrease was observed in both photosynthetic efficiency(α) and F_v/F_m. At the same time, $rETR_{max}$ and E_k increased due to a lowered α (Fig. 4). This corresponded to a phytoplankton community shift in which the growth of practically all groups declined except for dinoflagellates and *E. huxleyi*. During Days 11−22, high dFe (+DFB) promoted a significant increase in F_v/F_m with respect to the control (LC−DFB), and also an increase in α at the expense of a constant $rETR_{max}$. F_v/F_m values and growth rates are in agreement with those observed for *E. huxleyi* cultures grown under different Fe conditions at ambient CO_2 (Honey et al. 2013). The F_v/F_m decay under Fe stress is a widely observed response (Behrenfeld & Milligan 2013), as the photosynthetic electron transport chain is the primary control on cell growth under low Fe conditions.

Thus, the higher *E. huxleyi* growth rates of 0.61 d^{-1} observed under elevated dFe levels (+DFB) vs. 0.52 d^{-1} at ambient dFe (−DFB) (Segovia et al. 2017) are due to the increase in pigment ratios and the values of the photosynthetic parameters. In contrast, growth rates were significantly lower in HC (0.35 d^{-1} average) than in LC treatments, matching lower F_v/F_m (0.48 average) and α values found at high CO_2 levels. The inability to sustain high operative photosynthetic electron transport rates and cell division at increased CO_2 is most likely due to the inability of the cells to regulate the internal pH. Maintaining a constant intracellular pH is energetically costly, and ocean acidification likely affects the cellular energy demands (Taylor et al. 2012). Additionally, a probable decrease in calcification under high CO_2 (Gao et

al. 2009, Xu et al. 2011, Mackey et al. 2015) makes the cell prone to photoinhibition due to the inability of managing a high irradiance dose (see Table 1). Indeed, cells showed decreased photosynthetic parameters and were unable to grow.

It is expected that a photophysiologically stressed cell (by both the lack of Fe required to meet the cell quotas or by an excess of CO_2, i.e. lower pH) produces ROS. Such ROS can be directly produced by the harming effects of excess light reaching the cell due to altered pigment content (by decreasing the size of the sink of photosynthetically produced electrons). Also, ROS can be indirectly produced, due to chemical, physical or photosensitised reactions inside and outside the cells (Lesser 2006). This can ultimately lead to cell death (Segovia & Berges 2009, Bouchard et al. 2013, Sobrino et al. 2014). Strikingly, cell death was only detected during the shift in the phytoplankton community structure between Days 10 and 12, coincident with a decrease in F_v/F_m and α, and not when the bloom of large-chain diatoms was crashing in Phase 1, or when some of the phytoplankton groups declined in Phase 2. A possible explanation is that a dead cell persists for a very short time in a natural plankton community, where there is high grazing pressure and bacterial remineralisation. Indeed, Segovia et al. (2017) reported that in this experiment, small autotrophs were efficiently grazed by microzooplankton, which in turn were probably consumed by copepods. Another possibility is that cellular ROS-detoxification and repair processes were highly effective, and ROS production also correlated with growth metabolism, similarly to other metabolic and enzymatic activities under non-stressful conditions (Sobrino et al. 2014). A ROS signal was also detected on Days 10–16 in parallel with cell death. Greater oxidative stress was observed in –DFB treatments, but it was buffered when dFe increased. The fact that LC+DFB treatments showed significantly higher ROS fluorescent signal than HC+DFB also points towards a more active metabolism producing ROS, in agreement with higher α and F_v/F_m and most likely due to a higher photosynthetic rate (Lorenzo et al. 2017). Furthermore, ca. 80% of cells were not ROS stained, indicating that oxidative stress was very low, or basal, in the treatments. This seems to be in accordance with the lack of other symptoms of stress such as the production of dimethylsulphoniopropionate by the coccolithophore during the experiment (M. Mausz pers.comm.). Cellular repair processes depend on energy supply (ATP and NADPH), nitrogen and phosphorus for protein and nucleic acid synthesis. Thus, the final cell response showcases the balance between cellular damage and repair, and likely depends on nutrient availability (Litchman et al. 2002). *E. huxleyi* outcompetes other phytoplankton at high N:P ratios compared to low N:P ratios, it exploits organic nutrients successfully, it is not photoinhibited at high irradiances, and it has fast growth rates (Paasche 2001), thriving under ambient CO_2 scenarios. Macronutrient concentrations in the present study were low. Phytoplankton growth during Phase 2 was sustained on ammonia (Segovia et al. 2017), and the cells' stoichiometric requirements were fulfilled. However, dFe was insufficient to support the Fe demand of *E. huxleyi* at ambient conditions (LC–DFB), leading to impaired growth rates. Fe is not only essential in photosynthesis and respiration, but it is also the cofactor of many proteins that participate in other cellular processes ensuring cellular viability and growth, such as the proteins

involved in DNA repair and ROS scavenging (Lukianova & David 2005, Morita et al. 2010, Twining & Baines 2013).

Ocean acidification decreases calcification (Riebesell & Tortell 2011), producing malformed coccoliths, therefore increasing the impact of high PAR, UVA and UVB irradiances in the cell (Gao et al. 2009). Under such conditions, higher DNA damage by means of CPD accumulation would be expected in the HC treatments, due to higher biologically effective UVR dose (Table 1). Remarkably, once Phase 2 was well established (Days 12–22), the concentration of CPDs was significantly higher in the control (LC–DFB) than in any of the other treatments after Day 11 (Fig. 5, Table 2). DNA lesions were minimised by high dFe, either promoted by the addition of DFB alone (LC+DFB), by increased CO_2, (HC–DFB) or by both (HC+DFB). The high CPD accumulation in HC–DFB on Day 21 was most likely due to small and large nanoeukaryotes and dinoflagellates dominating the community (in agreement with photosynthetic parameters). This was the only treatment where *E. huxleyi* was outnumbered by other groups, including prasinophytes, single-celled diatoms and dinoflagellates, that proved not to be affected by elevated CO_2 but that are reported to be highly sensitive to UVR (Bouchard et al. 2013, Sobrino et al. 2014). In any case, LC+DFB was the treatment that presented the lowest CPD concentration (Fig. 6). Photolyase (PL) is the enzyme that cleaves the cyclobutane ring of the pyrimidine dimer in a process called 'photo-reactivation' (Sancar 1994). While most DNA damage products are repaired via a variety of 'remove and replace' (nucleotide excision and base excision repair) mechanisms, pyrimidines are repaired directly by photolyases (Britt 2004). The PL-mediated photo-reactivation process was demonstrated in several species of phytoplankton (Buma et al. 2000, Boelen et al. 2001, Yi et al. 2006, Heijde et al. 2010, Brazard et al. 2012, García-Gómez et al. 2014, 2016). Photolyase harnesses blue or near-UV light energy to cleave the cyclobutane ring of the pyrimidine dimer (Stuchebrukhov 2011), thus preventing the harmful effects of UV radiation. Photolyase activation might possibly be related to an increase in absorption in the blue wavelength by chl c_3 in *E. huxleyi* (Mizoguchi et al. 2011), given that this pigment increased significantly during the bloom and both dFe and CO_2, as well as their interaction, had significant effects on its accumulation (Fig. 2, Table 2).

This is the first time that CPD accumulation subjected to multiple stressors other than UVR is reported in *E. huxleyi*. Our results indicate that the response of *E. huxleyi* to ambient UVR is dependent on Fe and modulated by CO_2, as well as that natural levels of UVR are able to cause harmful effects in this species; thus, the already known tolerance of this species to high irradiance (Paasche 2001) might depend on other factors. CPDs bring both DNA and RNA polymerases to a standstill and may result in mutations or cell death. If DNA repair is effective, then cell survival is high and cell stress due to the oxidative burst decreases as a consequence of the transcription of genes encoding for enzymes involved in ROS scavenging (superoxide dismutase, catalases, ascorbate peroxidases, glutathione reductase) being transcribed, as well as other genes necessary for cell functioning, as demonstrated for other species (García-Gómez et al. 2016). A principal component analyses was carried out in order to detect trends that were not obvious, but it did

not reveal any new findings (data not shown); thus, we conclude that Fe is needed for DNA repair and to overcome oxidative stress in *E. huxleyi*.

Fe might also be directly required to cope with environmental stress, because a large number of proteins have this metal as a cofactor, being a compulsory requisite for catalyses. The presence of genes encoding for Fe-metalloproteins in the *E. huxleyi* genome (Read et al. 2013) might provide further evidence for the importance of Fe in the stress response of this coccolithophore.

CONCLUSIONS

Emiliania huxleyi experienced Fe limitation under ambient dFe conditions (−DFB). However, increased dFe (+DFB) partially mitigated the negative effect of elevated CO_2 inflicted on the coccolithophore (Segovia et al. 2017). This indicates a physiological Fe-mediated acclimation response to ocean acidification by this species. The stress response demonstrated in this study further supports this finding, adding evidence for an important role of Fe in the physiology of *E. huxleyi*: (1) increased dFe favoured the accumulation of key pigments and modulated the physiological response depending on pCO_2 levels; (2) changes in photosynthetic parameters were directly related to trends in accessory pigments; (3) the threshold ROS levels corresponded to normal metabolism, most likely suggesting an efficient detoxifying mechanism; and (4) DNA damage was minimised by increased dFe. Fe might also be indirectly needed to fulfil the energy requirements imposed by the proteins involved in such processes, and that is not supplied under ambient dFe due to limitation, or that is diminished due to the negative effect of ocean acidification on cell physiology.

Within the future predicted global scenario for coastal ecosystems, phytoplankton will experience a more acidic ocean. It will also be exposed to higher irradiances as a consequence of a shallower thermocline, and nutrients will be most likely limiting (Doney et al. 2009). However, particulate and/or colloidal Fe might become more solubilised by lower pH, and organic ligands might also be photosolubilised due to increased UVR (Segovia et al. 2017 and references therein). This will impact globally important species such as *E. huxleyi*, leading to diverse ecological consequences. *E. huxleyi* strains able to thrive in the presence of a factor such as dFe, which comes into play as a result of the novel scenario, would become more competitive. The balance between the organic carbon pump and the carbonate counter pump (Rost & Riebesell 2004) could be affected, modifying the net downward particulate organic carbon flux, and the CO_2 interchange between the ocean and the atmosphere, and thus, carbon cycling. All of these results taken together provide evidence that studying the interactive effects between different global-change-driven factors is crucial to be able to understand and predict how the future ocean can be affected.

Acknowledgements. This work was funded by CTM/MAR 2010-17216 (PHYTOSTRESS) research grant from the Spanish Ministry for Science and Innovation (Spain) to M.S., M.R.L. and C.I. were funded by FPU grants from the

Ministry for Education (Spain). We thank María T. Maldonado for discussions and the rest of the PHYTOSTRESS team for collaboration and help.

LITERATURE CITED

Beardall J, Stojkovic S, Larsen S (2009) Living in a high CO_2 world: impacts of global climate change on marine phytoplankton. Plant Ecol Divers 2: 191–205

Beaufort L, Probert I, de Garidel-Thoron T, Bendif EM and others (2011) Sensitivity of coccolithophores to carbonate chemistry and ocean acidification. Nature 476: 80–83

Behrenfeld MJ, Milligan AJ (2013) Photophysiological expressions of iron stress in phytoplankton. Annu Rev Mar Sci 5: 217–246

Boelen P, Veldhuis MJW, Buma AGJ (2001) Accumulation and removal of UVBR induced DNA damage in marine tropical plankton subjected to mixed and simulated nonmixed conditions. Aquat Microb Ecol 24: 265–274

Bouchard JN, García-Gómez C, Lorenzo MR, Segovia M (2013) Differential effect of ultraviolet exposure (UVR) in the stress response of the Dinophycea *Gymnodinium* sp. and the Chlorophyta *Dunaliella tertiolecta*: mortality versus survival. Mar Biol 160: 2547–2560

Boyd PW, Doney SC (2002) Modelling regional responses by marine pelagic ecosystems to global climate change. Geophys Res Lett 29: 53-1–53-4

Brazard J, Ley C, Lacombat F, Plaza P and others (2012) Photo antenna in two cryptochrome–photolyase proteins from *O. tauri*: presence, nature and ultrafast photoinduced dynamics. J Photochem Photobiol Chem 234:135–145

Breitbarth E, Bellerby RJ, Neill CC, Ardelan MV and others (2010) Ocean acidification affects iron speciation during a coastal seawater mesocosm experiment. Biogeosciences 7: 1065–1073

Britt AB (2004) Repair of DNA damage induced by solar UV. Photosynth Res 81: 105–112

Buma AG, Van Oijen T, Van De Poll W, Veldhuis MJW, Gieskes WWC (2000) The sensitivity of *Emiliania huxleyi* (Prymnesiophyceae) to ultraviolet-B radiation. J Phycol 36: 296–303

Caldwell M (1971) Solar UV irradiance and the growth and development of higher plants. Photophysiology 4: 131–177

Ciais P, Sabine C, Bala G, Bopp L and others (2013) Carbon and other biogeochemical cycles. In: Stocker TF, Qin D, Plattner GK, Tignor M and others (eds) Climate change 2013: the physical science basis. Contribution of Working Group I to the Fifth Assessment Report of the Intergovernmental Panel on Climate. Cambridge University Press, Cambridge, p 465–570

Cullen J, Neale P (1997) Biological weighting functions for describing the effects of ultraviolet radiation on aquatic systems. In: Häder DP (ed) The effects of ozone depletion on aquatic ecosystems. RG Landes, Austin, TX, p 97–118

Cullen JJ, Neale PJ, Lesser MP (1992) Biological weighting function for the inhibition of phytoplankton photosynthesis by ultraviolet radiation. Science 258: 646–650

Demmig-Adams B, Adams WW (1996) Xanthophyll cycle and light stress in nature: uniform response to excess direct sunlight among higher plant species. Planta 198: 460–470

Doney SC, Fabry VJ, Feely RA, Kleypas JA (2009) Ocean acidification: the other CO_2 problem. Annu Rev Mar Sci 1: 169–192
Egge JK, Heimdal BR (1994) Blooms of phytoplankton including *Emiliania huxleyi* (Haptophyta). Effect of nutrient supply in different N:P ratios. Sarsia 79: 333–348
Eilers PHC, Peeters JCH (1988) A model for the relationship between light intensity and the rate of photosynthesis in phytoplankton. Ecol Model 42: 199–215
Endo H, Yoshimura T, Kataoka T, Suzuki K (2013) Effects of CO_2 and iron availability on phytoplankton and eubacterial community compositions in the northwest subarctic Pacific. J Exp Mar Biol Ecol 439: 160–175
Endo H, Hattori H, Mishima T, Hashida G, Sasaki H, Nishioka J, Suzuki K (2017) Phytoplankton community responses to iron and CO_2 enrichment in different biogeochemical regions of the Southern Ocean. Polar Biol 40: 2143–2159
Figueroa FL, Korbee N, Carrillo P, Medina-Sánchez JM, Mata MT, Bonomi J, Sánchez-Castillo PM (2009) The effects of UV radiation on photosynthesis estimated as chlorophyll fluorescence in *Zygnemopsis decusata* (Chlorophyta) growing in a high mountain lake (Sierra Nevada, Southern Spain). J Limnol 68: 206–216
Gao K, Ruan Z, Villafañe VE, Gattuso JP, Helbling EW (2009) Ocean acidification exacerbates the effect of UV radiation on the calcifying phytoplankter *Emiliania huxleyi*. Limnol Oceanogr 54: 1855–1862
García-Gómez C, Parages ML, Jimenez C, Palma A, Mata MT, Segovia M (2012) Cell survival after UV radiation stress in the unicellular chlorophyte *Dunaliella tertiolecta* is mediated by DNA repair and MAPK phosphorylation. J Exp Bot 63: 5259–5274
García-Gómez C, Gordillo FJL, Palma A, Lorenzo MR, Segovia M (2014) Elevated CO_2 alleviates high PAR and UV stress in the unicellular chlorophyte *Dunaliella tertiolecta*. Photochem Photobiol Sci 13: 1347–1358
García-Gómez C, Mata MT, Van Breusegem F, Segovia M (2016) Low-steady-state metabolism induced by elevated CO_2 increases resilience to UV radiation in the unicellular green-algae *Dunaliella tertiolecta*. Environ Exp Bot 132: 163–174
Häder DP, Kumar HD, Smith RC, Worrest RC (1998) Effects on aquatic ecosystems. J Photochem Photobiol B 46: 53–68
Hammer Ø, Harper DAT, Ryan PD (2001) PAST: paleontological statistics software package for education and data analysis. Palaeontol Electron 4: art4
Heijde M, Zabulon G, Corellou F, Ishikawa T and others (2010) Characterization of two members of the cryptochrome/photolyase family from *Ostreococcus tauri* provides insights into the origin and evolution of cryptochromes. Plant Cell Environ 33: 1614–1626
Honey DJ, Gledhill M, Bibby TS, Legiret FE and others (2013) Heme b in marine phytoplankton and particulate material from the North Atlantic Ocean. Mar Ecol Prog Ser 483: 1–17
Hutchins DA (2011) Forecasting the rain ratio. Nature 476:41–42
Jakobsen HH, Carstensen J (2011) FlowCAM: sizing cells and understanding the impact of size distributions on biovolume of planktonic community structure. Aquat Microb Ecol 65: 75–87
Jones LW, Kok B (1966) Photoinhibition of chloroplast reactions. I. Kinetics and action spectra. Plant Physiol 41:1037–1043

Kuma K, Nishioka J, Matsunaga K (1996) Controls on iron(III) hydroxide solubility in seawater: the influence of pH and natural organic chelators. Limnol Oceanogr 41: 396–407
Larsen A, Castberg T, Sandaa RA, Brussaard CPD and others (2001) Population dynamics and diversity of viruses, bacteria and phytoplankton in a shallow eutrophic lake. Mar Ecol Prog Ser 221: 47–57
Lesser MP (2006) Oxidative stress in marine environments: biochemistry and physiological ecology. Annu Rev Physiol 68: 253–278
Litchman E, Neale PJ, Banaszak AT (2002) Increased sensitivity to ultraviolet radiation in nitrogen-limited dinoflagellates: photoprotection and repair. Limnol Oceanogr 47: 86–94
Lorenzo MRL, Iñiguez C, Egge J, Larsen A, Berger SAB, Garcia-Gomez C, Segovia M (2017) Increased CO_2 and iron availability effects on carbon assimilation and calcification on the formation of *Emiliania huxleyi* blooms in a coastal phytoplankton community. Environ Exp Bot, doi. org/ 10. 1016/ j. envexpbot. 2017. 12.003
Lubian LM, Montero O (1998) Excess light-induced violaxanthin cycle activity in *Nannochloropsis gaditana* (Eustigmatophyceae): effects of exposure time and temperature. Phycologia 37: 16–23
Lukianova OA, David SS (2005) A role for iron-sulfur clusters in DNA repair. Curr Opin Chem Biol 9: 145–151
Mackey KRM, Morris JJ, Morel FMM, Kranz SA (2015) Response of photosynthesis to ocean acidification. Oceanography 28: 74–91
Marchetti A, Maldonado MT (2016) Iron. In: Borowitzka MA, Beardall J, Raven JA (eds) The physiology of microalgae. Springer International Publishing, Cham
Marie D, Brussaard CPD, Thyrhaug R, Bratbak G, Vaulot D (1999) Enumeration of marine viruses in culture and natural samples by flow cytometry. Appl Environ Microbiol 65: 45–52
Menden-Deuer S, Lessard EJ (2000) Carbon to volume relationships for dinoflagellates, diatoms, and other protist plankton. Limnol Oceanogr 45: 569–579
Millero FJ, Woosley R, Ditrolio B, Waters J (2009) Effect of ocean acidification on the speciation of metals in seawater. Oceanography 22: 72–85
Mizoguchi T, Kimura Y, Yoshitomi T, Tamiaki H (2011) The stereochemistry of chlorophyll-c_3 from the haptophyte *Emiliania huxleyi*: The (132R)-enantiomers of chlorophylls-*c* are exclusively selected as the photosynthetically active pigments in chromophyte algae. Biochim Biophys Acta 1807: 1467–1473
Morita R, Nakane S, Shimada A, Inoue M and others (2010) Molecular mechanisms of the whole DNA repair system: a comparison of bacterial and eukaryotic systems. J Nucl Acids 2010: 179594
Muggli DL, Harrison PJ (1996) Effects of nitrogen source on the physiology and metal nutrition of *Emiliania huxleyi* grown under different iron and light conditions. Mar Ecol Prog Ser 130: 255–267
Olenina I, Hajdu S, Edler L, Wasmund N and others (2006) Biovolumes and size-classes of phytoplankton in the Baltic Sea. Baltic Sea Environment Proceedings No. 106.Helsinki Commission, Baltic Marine Environment Protection Commission, Helsinki

Öztürk M, Steinnes E, Sakshaug E (2002) Iron speciation in the Trondheim Fjord from the perspective of iron limitation for phytoplankton. Estuar Coast Shelf Sci 55: 197–212
Paasche E (2001) A review of the coccolithophorid *Emiliania huxleyi* (Pymnesiophyceae), with particular reference to growth, coccolith formation, and calcification-photosynthesis interactions. Phycologia 40: 503–529
Polimene L, Brunet C, Allen JI, Butenschon M, White DA, Llewellyn CA (2012) Modelling xanthophyll photoprotective activity in phytoplankton. J Plankton Res 34: 196–207
Read BA, Kegel J, Klute MJ, Kuo A and others (2013) Pangenome of the phytoplankton *Emiliania* underpins its global distribution. Nature 499: 209–213
Riebesell U, Gattuso JP (2015) Lessons learned from ocean acidification research. Nat Clim Chang 5: 12–14
Riebesell U, Tortell PD (2011) Effects of ocean acidification on pelagic organisms and ecosystems. In: Gatusso JP, Lansson L (eds) Ocean acidification. Oxford University Press, Oxford, p 99–121
Riebesell U, Bellerby RGJ, Grossart HP, Thingstad F (2008) Mesocosm CO_2 perturbation studies: from organism to community level. Biogeosciences 5: 1157–1164
Rost B, Riebesell U (2004) Coccolithophores and the biological pump: responses to environmental changes. In: Thierstein HR, Young JR (eds) Coccolithophores: from molecular process to global impact. Springer, Berlin, p 99–125
Sabine CL, Feely RA, Gruber N, Key RM and others (2004) The oceanic sink for anthropogenic CO_2. Science 305: 367–371
Sancar A (1994) Structure and function of DNA photolyase. Biochemistry 33: 2–9
Schulz KG, Riebesell U (2013) Diurnal changes in seawater carbonate chemistry speciation at increasing atmospheric carbon dioxide. Mar Biol 160: 1889–1899
Schulz KG, Ramos JB, Zeebe RE, Riebesell U (2009) CO_2 perturbation experiments: similarities and differences between dissolved inorganic carbon and total alkalinity manipulations. Biogeosciences 6: 2145–2153
Segovia M, Berges JA (2009) Inhibition of caspase-like activities prevents the appearance of reactive oxygen species and dark-induced apoptosis in the unicellular chlorophyte *Dunaliella tertiolecta*. J Phycol 45: 1116–1126
Segovia M, Mata T, Palma A, García-Gómez C, Lorenzo R, Rivera A, Figueroa FL (2015) *Dunaliella tertiolecta* (Chlorophyta) avoids cell death under ultraviolet radiation by triggering alternative photoprotective mechanisms. Photochem Photobiol 91: 1389–1402
Segovia M, Lorenzo MR, Maldonado MT, Larsen A and others (2017) Iron availability modulates the effects of future CO_2 levels within the marine planktonic food web. Mar Ecol Prog Ser 565: 17–33
Setlow RB (1974) The wavelengths in sunlight effective in producing skin cancer: a theoretical analysis. Proc Natl Acad Sci USA 71: 3363–3366
Shi D, Xu Y, Hopkinson BM, Morel FMM (2010) Effect of ocean acidification on iron availability to marine phytoplankton. Science 327: 676–679
Sobrino C, Segovia M, Neale PJ, Mercado JM and others (2014) Effect of CO_2, nutrients and light on coastal plankton. IV. Physiological responses. Aquat Biol 22: 77–93

Stocker TF, Qin D, Plattner GK, Tignor M and others (eds) (2013) Climate change 2013: the physical science basis. Contribution of Working Group I to the Fifth Assessment Report of the Intergovernmental Panel on Climate Change. Cambridge University Press, Cambridge
Stolte W, Kraay GW, Noordeloos AAM, Riegman R (2000) Genetic and physiological variation in pigment composition of Emiliania huxleyi (Prymnesiophyceae) and the potential use of its pigment ratios as a quantitative physiological marker. J Phycol 36: 529–539
Stuchebrukhov A (2011) Watching DNA repair in real time. Proc Natl Acad Sci USA 108: 19445–19446
Suffrian K, Simonelli P, Nejstgaard JC, Putzeys S, Carotenuto Y, Antia AN (2008) Microzooplankton grazing and phytoplankton growth in marine mesocosms with increased CO_2 levels. Biogeosciences 5: 1145–1156
Sugie K, Endo H, Suzuki K, Nishioka J, Kiyosawa H, Yoshi mura T (2013) Synergistic effects of pCO_2 and iron availability on nutrient consumption ratio of the Bering Sea phytoplankton community. Biogeosciences 10: 6309–6321
Takaichi S (2001) Carotenoids in algae: distributions, biosyntheses and functions of carotenoids in algae. Mar Drugs 9: 1101–1118
Taylor AR, Brownlee C, Wheeler GL (2012) Proton channels in algae: reasons to be excited. Trends Plant Sci 17: 675–684
Twining BS, Baines SB (2013) The trace metal composition of marine phytoplankton. Annu Rev Mar Sci 5: 191–215
Veldhuis M, Kraay G, Timmermans K (2001) Cell death in phytoplankton: correlation between changes in membrane permeability, photosynthetic activity, pigmentation and growth. Eur J Phycol 36: 167–177
Wellburn AR (1994) The spectral determination of chlorophylls *a* and *b*, as well as total carotenoids, using various solvents with spectrophotometers of different resolution. J Plant Physiol 144: 307–313
Wells ML (1999) Manipulating iron availability in nearshore waters. Limnol Oceanogr 44: 1002–1008
Xu K, Gao K, Villafañe VE, Helbling EW (2011) Photosynthetic responses of *Emiliania huxleyi* to UV radiation and elevated temperature: roles of calcified coccoliths. Biogeosciences 8: 1441–1452
Yi Y, Yi C, Qian L, Min L and others (2006) Cloning and sequence analysis of the gene encoding (6-4)photolyase from *Dunaliella salina*. Biotechnol Lett 28: 309–314

Table 1. Experimental irradiances, corresponding weighted irradiances (biological effective irradiance, BEI) and the biological effective dose (BED) in the control mesocosms on Day 6 (just before the addition of desferoxamine B [DFB] on Day 7), using the biologically effective 300 nm normalised weighting function for DNA damage (Setlow 1974), general plant damage (Caldwell 1971), inhibition of phytoplankton photosynthesis of *Phaeodactylum* (Cullen et al. 1992), inhibition of photosynthesis in Antarctic phytoplankton (Cullen & Neale 1997) and chloroplast inhibition (Jones & Kok 1966).

	Irradiance	
Experimental		
UVB (280–320 nm)	0.015 W m^{-2}	
UVA (320–400 nm)	2.057 W m^{-2}	
Photosynthetically active radiation (PAR, 400–700 nm)	180.97 µmol quanta m^{-2} s^{-1}	
Weighted	BEI (W m^{-2})	BED (KJ m^{-2})
DNA damage	0.0042	2.18
Generalised plant response	0.0039	2.05
Inhibition of *Phaeodactylum* photosynthesis	0.052	27.29
Inhibition of photosynthesis in Antarctic phytoplankton	0.09	49.49
Inhibition of photosynthesis of chloroplasts	0.37	191.68

Table 2. Statistical analyses (split-plot ANOVA) of the effects of CO_2, desferoxamine B (DFB) and their interaction, as well as the effect of time, on the variables analysed in the different treatments during Phase 2 (Days 11–22); $p < 0.05$ was considered significant; ns: not significant ($p > 0.05$). F_v/F_m: optimum quantum yield, α: photosynthetic efficiency, $rETR_{max}$: relative maximal electron transport rate, E_k: light saturation irradiance, PERI: peridinin, BUTA: 19'-butanoyloxyfucoxanthin, FUCO: fucoxanthin, HEXA: 19'-hexanoyloxyfucoxanthin, DD: diadinoxanthin, DT: diatoxanthin, Z: zeaxanthin, PRAS: prasinoxanthin, TFUCO: total fucoxanthin

Factor/variable	CO_2	DFB	Time	CO_2 × DFB	CO_2 × DFB × Time
F_v/F_m	<0.001	<0.001	<0.001	<0.05	<0.001
α	<0.01	ns	<0.005	<0.05	ns
E_k	ns	ns	ns	ns	ns
$rETR_{max}$	<0.05	ns	ns	ns	ns
Chl c_3	<0.001	<0.001	<0.05	<0.05	<0.05
Chl c_2	<0.01	ns	<0.001	ns	ns
PERI	<0.05	ns	<0.001	ns	ns
BUTA	<0.01	ns	<0.01	ns	ns
FUCO	<0.001	ns	<0.01	ns	ns
HEXA	<0.001	<0.001	<0.001	<0.001	<0.001
DD	<0.001	<0.001	<0.01	<0.01	ns
DT	<0.05	ns	<0.001	<0.05	<0.01
Z	<0.001	ns	<0.05	ns	ns
PRAS	<0.01	ns	<0.001	ns	ns
HEXA:FUCO	ns	<0.001	<0.001	<0.05	<0.001
DT+DD:TFUCO	ns	ns	<0.05	<0.001	<0.001
Cell death	<0.01	ns	<0.001	ns	ns
Oxidative stress	<0.01	ns	ns	ns	<0.05
DNA damage	ns	<0.001	<0.001	<0.05	<0.05

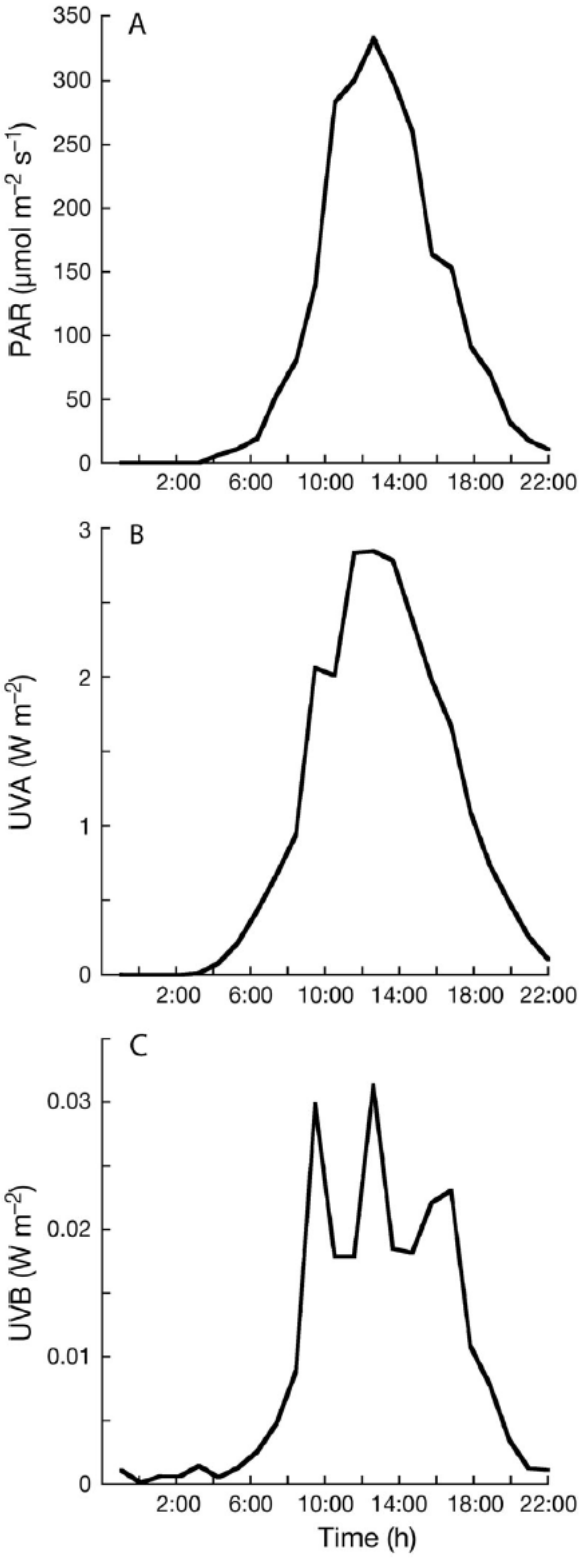

Figure 1. Experimental irradiances. (A) Photosynthetically active radiation (PAR), (B) UVA and (C) UVB in the control mesocosms on Day 6 (just before the addition of desferoxamine B [DFB] on Day 7).

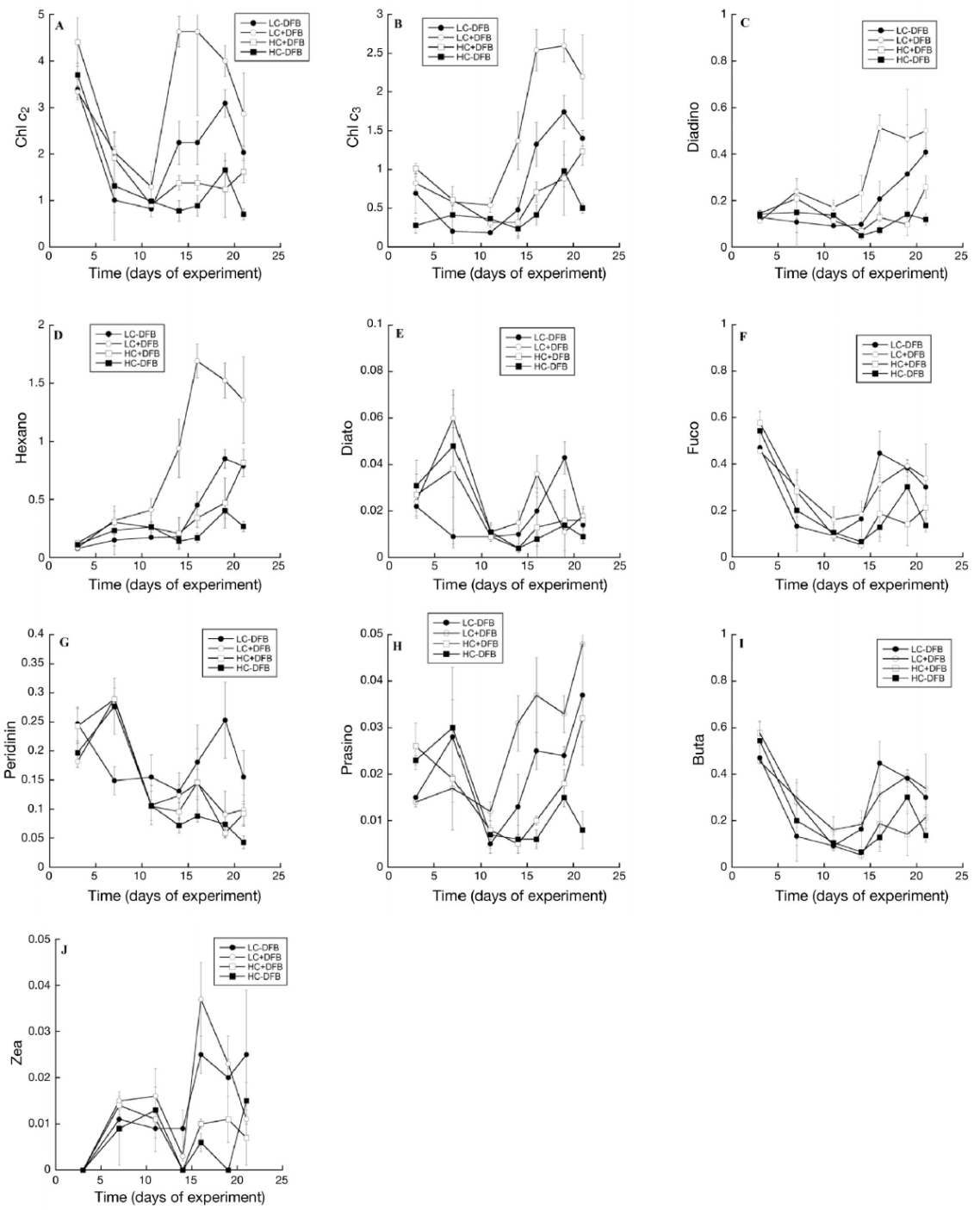

Figure 2. Temporal changes in pigment concentrations (µg l^{-1}) within the mesocosms: (A) chl c_2, (B) chl c_3, (C) diadinoxanthin, (D) 19'-hexanoyloxyfucoxanthin, (E) diatoxanthin, (F) fucoxanthin, (G) peridinin, (H) prasinoxanthin, (I) 19'-butanoyloxyfuco-xanthin and (J) zeaxanthin. Ambient (low) partial pressure of CO_2 (pCO_2) and ambient dissolved iron (dFe; LC−DFB [desferoxamine B], filled circles); ambient pCO_2 and increased dFe (LC+DFB, open circles); increased (high) pCO_2 and increased dFe (HC+DFB, open squares), increased pCO_2 and ambient dFe (HC−DFB, filled squares). Symbols indicate means of measurements in 3 independent mesocosms (n = 3) except for LC−DFB where n = 2. Error bars indicate standard deviations.

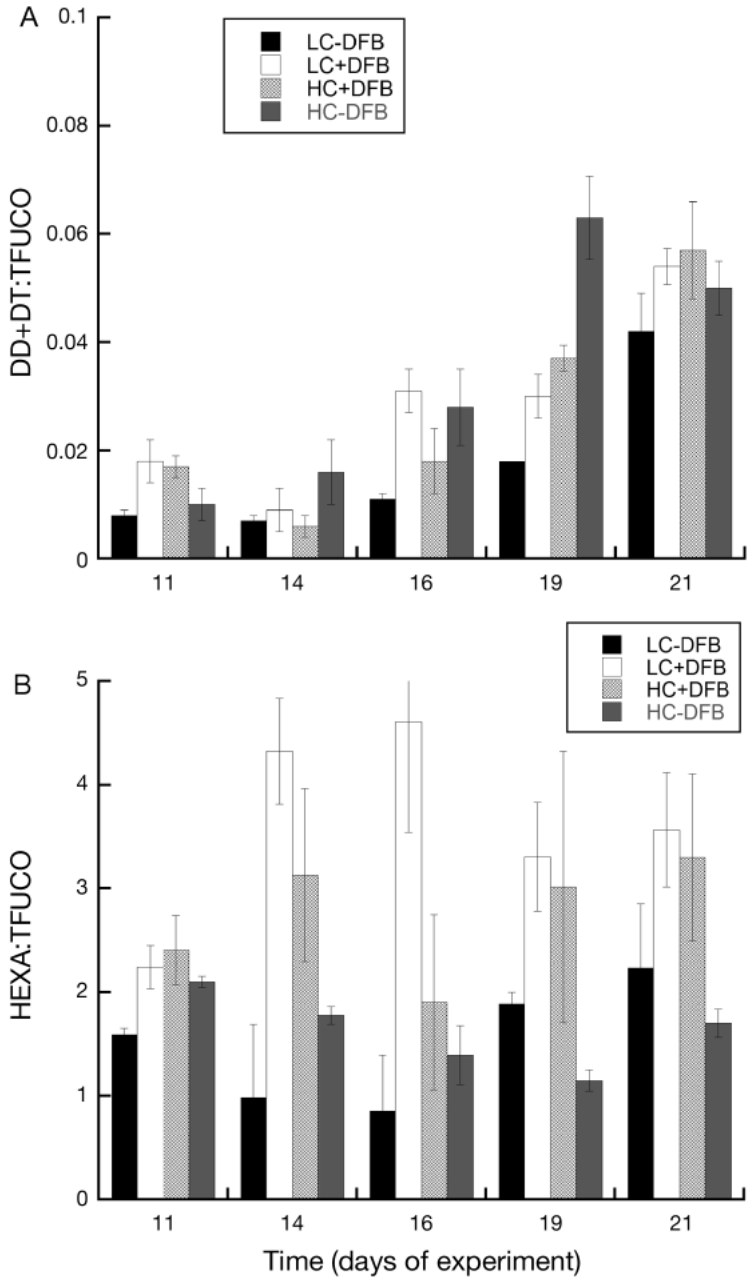

Figure 3. Ratios of (A) diatoxanthin and diadinoxantin to total fucoxanthins (DT+DD:TFUCO) and (B) 19'-hexanoyloxyfucoxanthin to total fucoxanthins (HEXA:TFUCO). Ambient partial pressure of CO_2 (pCO_2) and ambient dissolved iron (dFe; LC−DFB [desferoxamine B], black bars); ambient pCO_2 and increased dFe (LC+DFB, white bars); increased pCO_2 and increased dFe (HC+DFB, striped bars), increased pCO_2 and ambient dFe (HC−DFB, grey bars). Data are means of measurements in 3 independent mesocosms (n = 3) except for LC−DFB, where n = 2. Error bars indicate standard deviations.

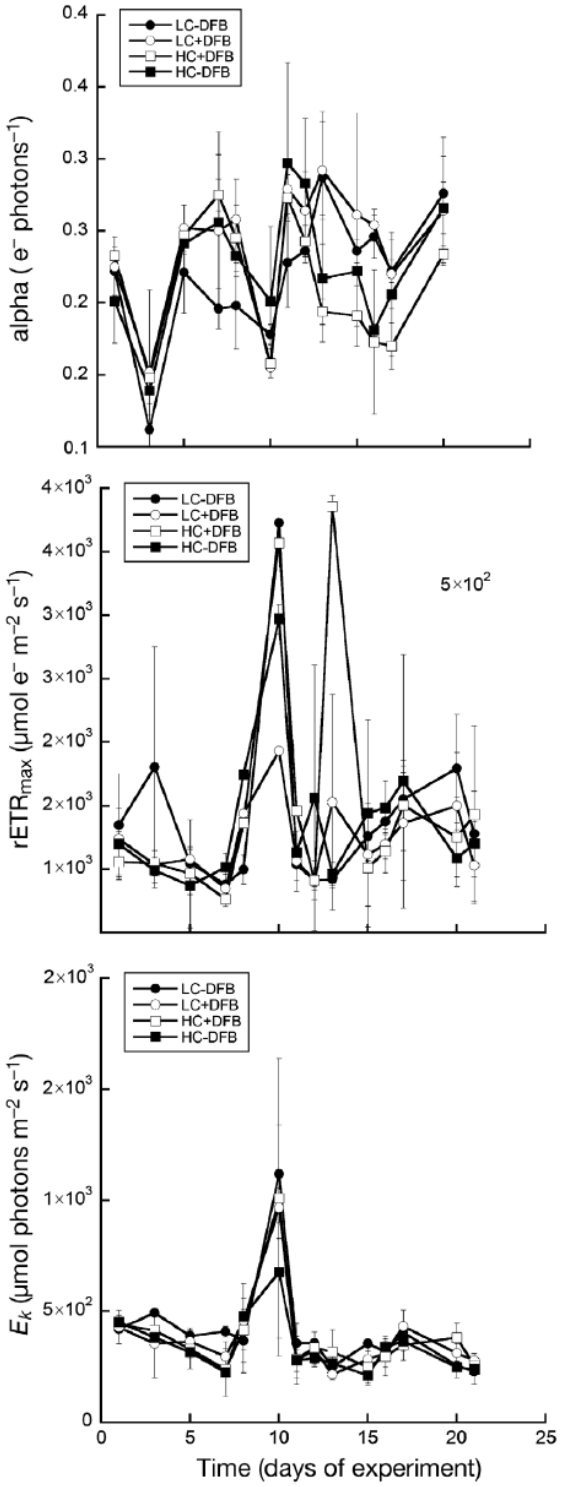

Figure 4. Temporal changes in the photosynthetic parameters: (A) photosynthetic efficiency (α), (B) relative maximal electron transport rate $rETR_{max}$ and (C) light saturation irradiance (E_k). Ambient partial pressure of CO_2 (pCO_2) and ambient dissolved iron (dFe; LC−DFB [desferoxamine B], filled circles); ambient pCO_2 and increased dFe (LC+DFB, open circles); increased pCO_2 and increased dFe (HC+DFB, open squares), increased pCO_2 and ambient dFe (HC−DFB, filled squares). Symbols indicate means of measurements in 3 independent mesocosms (n = 3) except for LC−DFB where n = 2. Error bars indicate standard deviations.

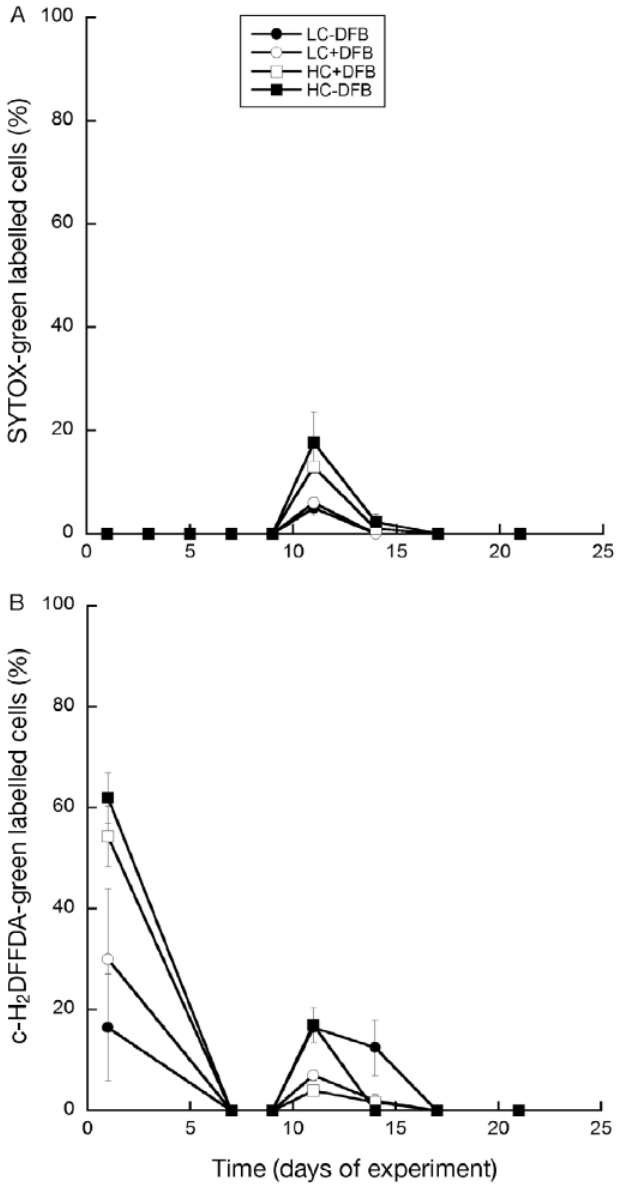

Figure 5. Temporal changes in (A) the percentage of dead cells (SYTOX-green labelled cells) and (B) the percentage of oxidative stress accumulation (c-H_2DFFDA-green labelled cells). Ambient partial pressure of CO_2 (pCO_2) and ambient dissolved iron (dFe; LC−DFB [desferoxamine B], filled circles); ambient pCO_2 and increased dFe (LC+DFB, open circles); increased pCO_2 and increased dFe (HC+DFB, open squares), increased pCO_2 and ambient dFe (HC−DFB, filled squares). Symbols indicate means of measurements in 3 independent mesocosms (n = 3) except for LC−DFB where n = 2. Error bars indicate standard deviations.

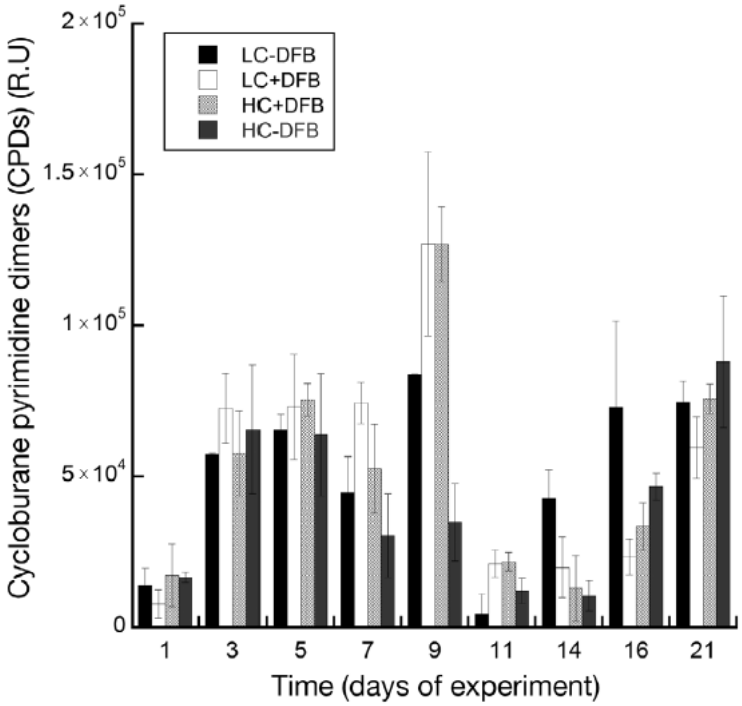

Figure 6. Temporal changes in DNA damage measured as cyclobutane pyrimidine dymers (CPDs) in the mesocosms. R.U.: relative units. Ambient partial pressure of CO_2 (pCO_2) and ambient dissolved iron (dFe; LC−DFB [desferoxamine B], black bars); ambient pCO_2 and increased dFe (LC+DFB, white bars); increased pCO_2 and increased dFe (HC+DFB, striped bars), increased pCO_2 and ambient dFe (HC−DFB, grey bars). Data are means of measurements in 3 independent mesocosms (n = 3) except for LC−DFB where n = 2. Error bars indicate standard deviations.